Adsorption (2011) 17:723–737
DOI 10.1007/s10450-011-9351-5

Improving the equilibrium performance of active carbons for separation processes by co-adsorption with low pressure solvent: application to carbon capture

Martin B. Sweatman

Received: 28 July 2010 / Accepted: 20 February 2011 / Published online: 22 March 2011

Abstract The equilibrium performance of a novel gas separation process described quite recently (Sweatman in Chem. Eng. Sci. 65:3907, 2010) called 'pressure-swing wetting layer absorption' here is investigated by means of molecular Monte-Carlo simulation. This process is very similar to pressure-swing adsorption except that solvent, in the form of low pressure vapour, is added to the gas to be separated in order to improve equilibrium performance. Earlier work, based on relatively simple density functional theory models, suggests that this process could be significantly more efficient than the analogous pressure-swing adsorption process when tetrahydrofuran (THF) is used as the solvent, although this conclusion is based only on equilibrium behaviour and does not take into account the effect of any dynamical processes. The aim of this work is to provide more detailed molecular simulation results to help understand this behaviour and guide experiments towards suitable solvents and conditions so that the process can experimentally tested. It is found that using acetonitrile as the solvent could be over nine times more effective than THF, which was modelled in previous work, for the particular carbon capture application studied here. These simulation results also demonstrate that, due to the effect of confinement on fluid structure, bulk solubility data cannot be used to reliably predict equilibrium performance in this context, and that the equilibrium performance is especially enhanced for pores that exhibit a bilayer phase transition.

Keywords Carbon capture · Porous media · Adsorption · Absorption · Molecular simulation · Monte-Carlo · Ternary mixture

M.B. Sweatman (✉)
Department of Chemical and Process Engineering, University of Strathclyde, Montrose Street, Glasgow G1 1XJ, UK
e-mail: martin.sweatman@strath.ac.uk

1 Introduction

Carbon capture and storage (CCS) is one option for reducing carbon dioxide emissions to the atmosphere. Its importance has been recognised by governments across the world, resulting in legislation in the UK at least. Unfortunately, carbon capture is also considered an expensive carbon abatement option, and so technologies that can dramatically reduce the costs of carbon capture are urgently needed.

This work seeks to further investigate a novel gas separation processes, called 'pressure-swing wetting layer *absorption*' here, in the context of carbon capture. This process was introduced in recent work (Sweatman 2010) referred to here as paper 1. Briefly, this process involves a porous material able to adsorb an absorbent fluid, which itself can selectively absorb the gas of interest, in this case carbon dioxide. A pressure-swing process is envisaged to recover the absorbed gas. The process must operate at subsaturated conditions with respect to the absorbent fluid so that both liquid-like and gas-like regions can exist simultaneously within the porous material. The liquid-like regions would have an effective gas-liquid interfacial area per cubic meter of absorption column many orders of magnitude times that of designs based on conventional packing materials. This huge increase in interfacial area could allow more compact process designs and consideration of more benign absorbents. Moreover, the process is not driven by gravity, as is the case with conventional absorption column designs, and so might be suited to mobile applications. For a carbon capture application, this process would almost certainly be required to operate with a vacuum swing, i.e. adsorption at about 1 bar and desorption at much lower pressure.

Paper 1 described and analysed this process from an equilibrium adsorption perspective using a simple density functional theory model. The main conclusion of that work was

that, compared to traditional pressure-swing adsorption (the same process, but without an absorbent solvent), the selectivity and capacity of a porous material could be significantly improved if the partial pressure of the solvent was carefully matched to the prevailing pore size. If the partial pressure of the solvent is too low then the solvent is hardly adsorbed and has little effect. On the other hand if the partial pressure of solvent is too high then the liquid-like regions formed within the smallest pores are too dense and essentially take no part in the separation process. However, for each pore size there is widow of opportunity, covering about a decade of pressure, within which both the selectivity and capacity of the gas to be separated are increased with respect to the case without solvent.

The aim of this work is to provide more detailed results than those in paper 1 to help understand this behaviour and guide experiments in the choice of suitable systems and conditions so that this process can be tested experimentally. Although the models and techniques in paper 1 are thought to reproduce the essential physics of fluids confined in nanopores, they are not sufficiently accurate to model and discriminate between several different solvents, and so they cannot be used to help guide experiments towards suitable test systems and conditions. Yet this is crucial for progress with the proposed novel process. Briefly, the DFT model in paper 1 employed simple spherical models of all molecules, together with straightforward density functional approximations to the respective statistical mechanical behaviour. This technique cannot be expected to reproduce the detailed behaviour of our ternary adsorption system that in reality is composed of highly non-spherical molecules in pores that have roughly the same dimension as the fluid molecules. Nor did the DFT model account in detail for electrostatic interactions (e.g. dipole-dipole and dipole-quadrupole) between fluid molecules that are thought to be important in determining performance. However, the kind of insight and detail required for comparison and guidance of experimental studies can be obtained my using molecular simulations, and so this work employs molecular Monte-Carlo simulations together with reasonably accurate molecular models.

The following sections describe results generated by molecular Monte-Carlo simulations of the adsorption of ternary fluid mixtures that aim to model carbon dioxide capture from an exhaust stream. The model systems are described in the next section. Results are obtained for several model solvents initially, and analysed to understand the basis of the observed phenomenon. Then, the best solvent from those tested is selected and results are obtained and analysed for a range of pore widths and exhaust gas pressures. The paper is concluded with a summary and discussion.

2 Simulation models and methods

The process outlined above and described in more detail in paper 1 is designed to separate carbon dioxide from an exhaust stream. The exhaust stream itself, for convenience and for comparison with earlier work, is taken to consist only of a binary mixture of nitrogen and carbon dioxide. Likewise, the same model pores are used in this work as in the earlier work, namely ideal graphitic slit-pores. These model pores are a convenient and, for some active carbons at least, a quite reasonable model of porosity. Although this model exhaust and porous material are very simple and neglect features that might be important actual applications, such as impurities in both the exhaust and adsorbent material, they are nevertheless thought to be sufficient to investigate the basic equilibrium performance of the process for a range of solvents and conditions.

2.1 Molecular models

As before, only physical organic solvents are considered in this work that aims to suggest suitable experimental test systems. In paper 1 tetrahydrofuran (THF) was selected as the solvent on the basis that experimental bulk absorption data (Fogg and Gerrard 1990a, 1990b) indicated it had good selectivity and capacity for carbon dioxide over nitrogen, while at the same time a suitable DFT model for THF could be developed. However, it was recognised in that work that the absorption behaviour of solvents in porous materials could be very different to their bulk behaviour due in part to the reduced dimensionality of the pore environment (i.e. due to confinement) and hence that selection on the basis of bulk behaviour is unlikely to lead to an optimal system. This indeed turns out to be true, and is demonstrated in the results section.

So, one of the first tasks of this work is to select a solvent on the basis of absorption behaviour under confinement. To this end, several solvents, namely acetonitrile, acetaldehyde, propane, dimethyl ether, acetone, methyl formate, THF, methyl acetate, diethyl ether and 3-pentanone, are modelled and simulated in graphitic slit-pores. Most molecular models are based on the TraPPE-UA molecular models of Seipmann and co-workers (Stubbs et al. 2004; Wick et al. 2005). These molecular models were designed and calibrated to be portable, i.e. they are considered to be general purpose models for use without further calibration. The ester models are based on the OPLS potentials of Briggs et al. (1991) which are calibrated to reproduce bulk liquid-state properties. The THF molecular model is based on that used by Zhao et al. (2006). Finally, carbon dioxide and nitrogen are also modelled in terms of TraPPE forcefields (Potoff and Siepmann 2001) (these models are calibrated to reproduce pure fluid vapour-liquid properties and

Table 1 Parameters for the molecular models used in this work. Symbols are described in the text

Molecule	LJ σ (nm)	LJ ε/k_B (K)	q (e)	Bond length	Bond angle
Nitrogen	N: 0.331	N: 36	N: −0.482	N–N: 0.11	N–q–N: 180°
	q-site: 0	q-site: 0	q-site: +0.964	N-q-site: 0.055	
Carbon dioxide	C: 0.27	C: 27.0	C: +0.7	C–O: 0.116	O–C–O: 180°
	O: 0.305	O: 79.0	O: −0.35		
Acetonitrile	CH_3: 0.375	CH_3: 98	CH_3: +0.269	CH_3–C: 0.154	CH_3–C–N: 180°
	C: 0.355	C: 60	C: +0.129	C–N: 0.1157	
	N: 0.295	N: 60	N: −0.398		
Acetaldehyde	CH_3: 0.375	CH_3: 98	CH_3: −0.043	CH–CH_3: 0.152	O–CH–CH_3: 121.4°
	CH: 0.352	CH: 54	CH: +0.525	CH–O: 0.1217	
	O: 0.305	O: 79	O: −0.482		
Propane	CH_3: 0.375	CH_3: 98	CH_3: 0	CH_3–CH_2: 0.154	CH_3–CH_2–CH_3: 114°
	CH_2: 0.395	CH_2: 46	CH_2: 0		
Dimethyl ether	CH_3: 0.375	CH_3: 98	CH_3: +0.25	CH_3–O: 0.141	CH_3–O–CH_3: 112°
	O: 0.28	O: 55	O: −0.5		
Acetone	CH_3: 0.375	CH_3: 98	CH_3: 0	CH_3–C: 0.152	CH_3–C=O: 121.4°
	C: 0.382	C: 40	C: +0.424	C=O: 0.1229	
	O: 0.305	O: 79	O: −0.424		
Methyl formate	CH_3: 0.38	CH_3: 85.58	CH_3: 0.25	CH_3–O: 0.1437	CH–O–CH_3: 115°
	CH: 0.375	CH: 57.86	CH: +0.55	CH=O: 0.12	O=CH–O: 125°
	O=: 0.296	O=: 105.72	O=: −0.4	CH–O: 0.1344	
	–O–: 0.3	–O–: 85.58	–O–: −0.4		
THF	CH_2: 0.43	CH_2: 45.28	CH_2: +0.28	CH_2–CH_2: 0.1523	CH_2–CH_2–CH_2: 101.4°
	O: 0.32	O: 100.62	CH_2(–O): −0.01	CH_2–O: 0.1432	CH_2–CH_2–O: 108°
			O: −0.54		CH_2–O–CH_2: 109.6°
Diethyl ether	CH_3: 0.375	CH_3: 98	CH_3: 0	CH_3–CH_2: 0.154	CH_3–CH_2–O: 112°
	CH_2: 0.395	CH_2: 46	CH_2: +0.25	CH_2–O: 0.141	CH_2–O–CH_2: 112°
	O: 0.28	O: 55	O: −0.5		
Methyl acetate	CH_3(–C): 0.391	CH_3(–C): 80.55	CH_3(–C): +0.05	CH_3–C: 0.152	CH_3–C=O: 125°
	CH_3(–O): 0.38	CH_3(–O): 85.58	CH_3(–O): +0.25	CH_3–O: 0.1437	CH_3–C–O: 110°
	C: 0.375	C: 57.86	C: +0.55	C=O: 0.12	CH_3–O–C: 115°
	O=: 0.296	O=: 105.72	O=: −0.45	C–O: 0.1344	
	–O–: 0.3	–O–: 85.58	–O–: −0.4		
3-Pentanone	CH_3: 0.375	CH_3: 98	CH_3: 0	CH_3–CH_2: 0.154	CH_3–CH_2–C: 114°
	CH_2: 0.395	CH_2: 46	CH_2: 0	CH_2–C: 0.152	CH_2–C–CH_2: 117.2°
	C: 0.382	C: 40	C: +0.424	C=O: 0.1229	CH_2–C=O: 121.4°
	O: 0.305	O: 79	O: −0.424		

properties of their mixtures with propane), and their details are also given in Table 1. All these molecular models consist of assemblies of Lennard-Jones (LJ) sites together with partial charges located on atom centres (except for nitrogen, which has an additional partial charge located in the middle of the double bond). So, the interaction energy between two molecules is given by

$$\phi = \sum_{ij} \left\{ 4\varepsilon_{ij} \left(\left(\frac{\sigma_{ij}}{r_{ij}} \right)^{12} - \left(\frac{\sigma_{ij}}{r_{ij}} \right)^{6} \right) + \frac{q_i q_j}{4\pi\varepsilon_0 r_{ij}} \right\} \quad (1)$$

where the sum is over all pairs of sites on different molecules, ε_{ij} and σ_{ij} are the LJ energy and size parameters

respectively for the interaction between sites i and j, q_i is the partial charge on site i, r_{ij} is the separation between the two sites, and ε_0 is the vacuum permittivity. Following the TraPPE convention LJ cross interactions are given by the Lorentz-Berthelot rules,

$$\sigma_{ij} = (\sigma_{ii} + \sigma_{jj})/2; \qquad \varepsilon_{ij} = \sqrt{\varepsilon_{ii}\varepsilon_{jj}} \tag{2}$$

Here, σ_{ii} and ε_{ii} are the LJ parameters for a particular LJ site. For simplicity, each model is taken here to be rigid and all except THF are coplanar, with a geometry corresponding to the lowest energy conformer of the TraPPE or OPLS models as appropriate. All model parameters are provided in Table 1. Unfortunately, a molecular model for methyl formate could not be found in the literature. To model this substance a molecular model is obtained based initially (see Table 1) on the OPLS model for methyl acetate (Briggs et al. 1991). On the basis of transferability, the methyl formate model is created by deleting the CH_3 group and adjusting slightly the partial charges on other groups. The resulting model is given in Table 1.

The interaction of each fluid component with a graphitic surface is modelled in terms of the Steele potential (Steele 1973)

$$V_i^s(z) = 2\pi\rho_s\Delta\sigma_{si}^2\varepsilon_{si} \times \left(\frac{2}{5}\left(\frac{\sigma_{si}}{z}\right)^{10} - \left(\frac{\sigma_{si}}{z}\right)^4 - \frac{\sigma_{si}^4}{3\Delta(0.61\Delta + z)^3}\right) \tag{3}$$

which depends only on the distance, z, of the LJ site from the surface. Here, ρ_s is the average density of carbon atoms in the surface, and Δ is the distance between graphene planes in a graphitic surface. Standard values (Sweatman and Quirke 2006) are used for these parameters ($\rho_s = 114$ nm^{-3}, $\Delta = 0.335$ nm). σ_{si} and ε_{si} are the length and energy parameters of the surface $-i$th site interaction. In this work these parameters are calculated using modified Lorentz-Berthelot rules

$$\sigma_{si} = (\sigma_{ii} + \sigma_s)/2; \qquad \varepsilon_{si} = k_{si}\sqrt{\varepsilon_{ii}\varepsilon_s} \tag{4}$$

where σ_s and ε_s are the length and energy LJ parameters respectively of the carbon atoms comprising the surface, while σ_{ii} and ε_{ii} are the respective LJ parameters of the ith fluid site. The usual values for the LJ parameters (Sweatman and Quirke 2006) are used in the work, i.e. $\sigma_s = 0.34$ nm and $\varepsilon_s/k_B = 28.0$ K. No attempt is made to calibrate solvent—wall interactions, primarily due to the lack of experimental data for these systems. On the other hand, carbon dioxide and nitrogen—wall interactions are calibrated to reproduce experimental adsorption data for several active carbons (Sweatman and Quirke 2005). Accordingly, the k_{si} parameter in (4) is set to 0.945 for all CO_2 site—wall interactions, while it is set to 1.0 for all other fluid site—wall interactions. The external potential generated by an ideal slit-pore is simply defined as

$$V_i^{ext}(z) = V_i^s(z) + V_i^s(H - z) \tag{5}$$

where H is the pore width.

2.2 Simulation methods

Standard grand canonical ensemble (μVT) molecular Monte-Carlo simulations (Frenkel and Smit 2002) are employed to determine equilibrium adsorption isotherms. In addition to standard translation-rotation, insertion and deletion moves, particle identity swap moves (Cracknell et al. 1993) are also performed when using the grand-canonical ensemble to improve sampling. All LJ pair-interactions are truncated without using long-range corrections at 2.5 nm, while the Ewald sum technique (Frenkel and Smit 2002) is employed to handle long-range electrostatic interactions using the same real-space cut-off. The 3-D periodic boundary technique of Yeh and Berkowitz (Frenkel and Smit 2002; Yeh and Berkowitz 1999) is used together with the Ewald sum technique for slit-pore simulations, with a separation of $5H$ between image slit-pores. Ewald sum parameters are chosen to produce errors in energy calculations of less than $0.001k_BT$. To achieve this, a routine for calculating the complementary error function is used that is everywhere accurate to at least 10 decimal places.

3 Results

The aim of this section is to investigate the equilibrium adsorption behaviour of model ternary systems comprising an organic solvent and the exhaust stream to be separated. Of particular interest is an understanding of which kinds of solvent show the most promise for this process, and why. Accordingly, Sect. 3.1 examines the equilibrium adsorption behaviour of ternary mixtures of the model exhaust gas and several different organic solvents. Later subsections examine the equilibrium adsorption behaviour of the most promising solvent obtained in Sect. 3.1 under different conditions. Section 3.2 examines the dependence of equilibrium adsorption on pore width, while Sect. 3.3 examines an increase in exhaust gas pressure.

In each case the focus is on the selectivity and capacity of carbon dioxide. Selectivity is a measure of the ability of the system to separate a gas mixture. Capacity is a crude measure of the volume of gas that can be treated by each cycle of the process. Both are important factors that influence process performance. The capacity of CO_2 is defined here as

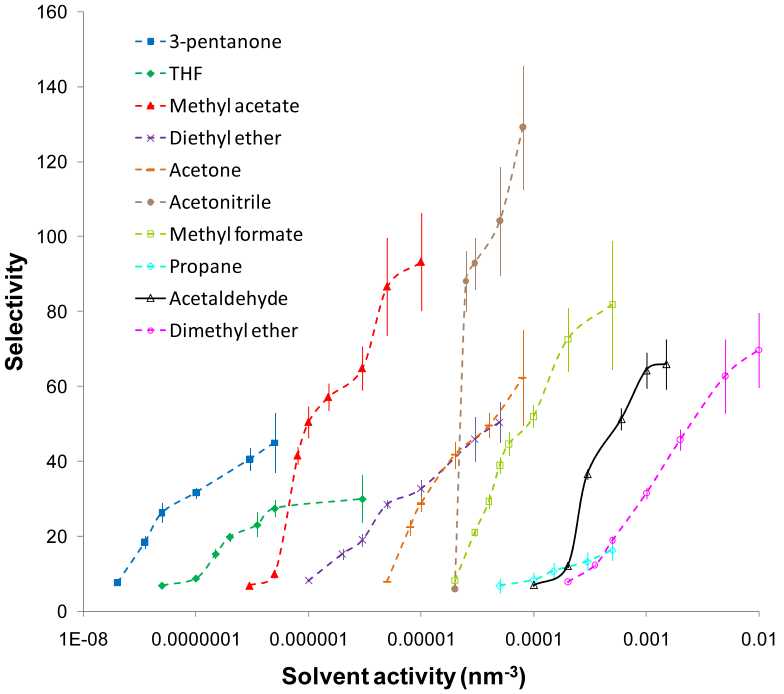

(a)

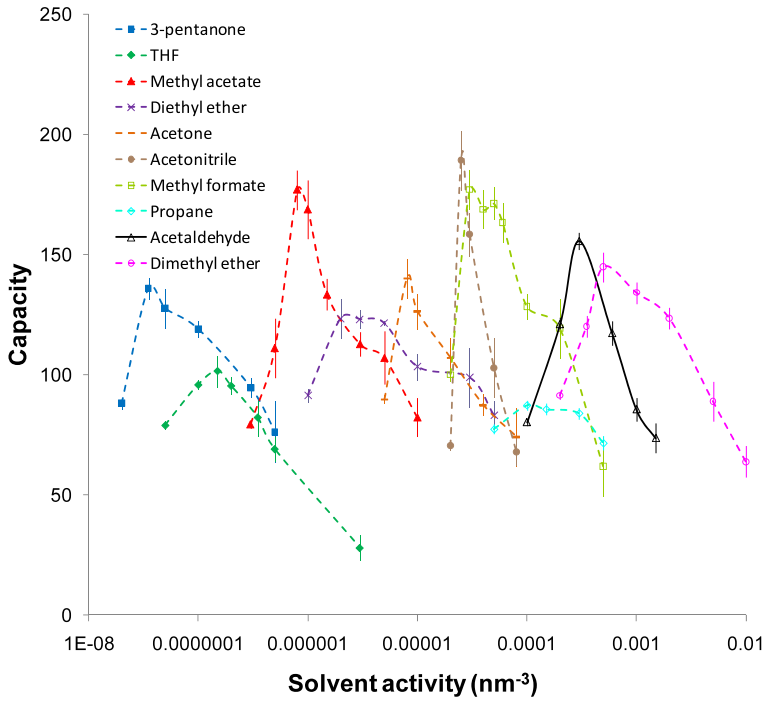

(b)

Fig. 1 (Color online) (**a**) Dependence of CO_2 selectivity (see text) on solvent activity for coadsorption of the solvent and exhaust gas in a 1 nm graphitic pore at 298.15 K. The solvents from left to right are 3-pentanone (*blue filled squares*), THF (*green filled diamonds*), methyl acetate (*red filled triangles*), diethyl ether (*purple crosses*), acetone (*orange horizontal bars*), acetonitrile (*brown filled circles*), methyl formate (*olive open squares*), propane (*cyan open diamonds*), acetaldehyde (*black open triangles*) and dimethyl ether (*pink open circles*). Solvent activity is plotted on a logarithmic scale. Symbols with error bars are simulation results while *dashed lines* are a guide. The solvent partial pressure (in bar), using the ideal gas law, is approximately 41.2 times the activity. (**b**) As for (**a**), except the CO_2 capacity (see text) is plotted. (**c**) As for (**a**), except the equilibrium performance (see text) is plotted. (**d**) As for (**a**), except the absolute specific solvent adsorption is plotted

$C_{CO_2} = \rho_{a,CO_2}/\rho_{b,CO_2}$, where ρ_{a,CO_2} is the average density of CO_2 adsorbed in the pore, i.e.

$$\rho_{a,CO_2} = \frac{1}{H}\int_0^H dz \rho_{CO_2}(z) \tag{6}$$

where $\rho_{CO_2}(z)$ is the density profile of CO_2 as a function of distance z across the slit-pore, and ρ_{b,CO_2} is the density of CO_2 in the bulk feed gas mixture. The selectivity of carbon dioxide is defined here simply as $S_{CO_2} = C_{CO_2}/C_{N_2}$. Taking the equilibrium performance to be linear in both the selectivity and capacity, another measure of performance, called

Fig. 1 (*Continued*)

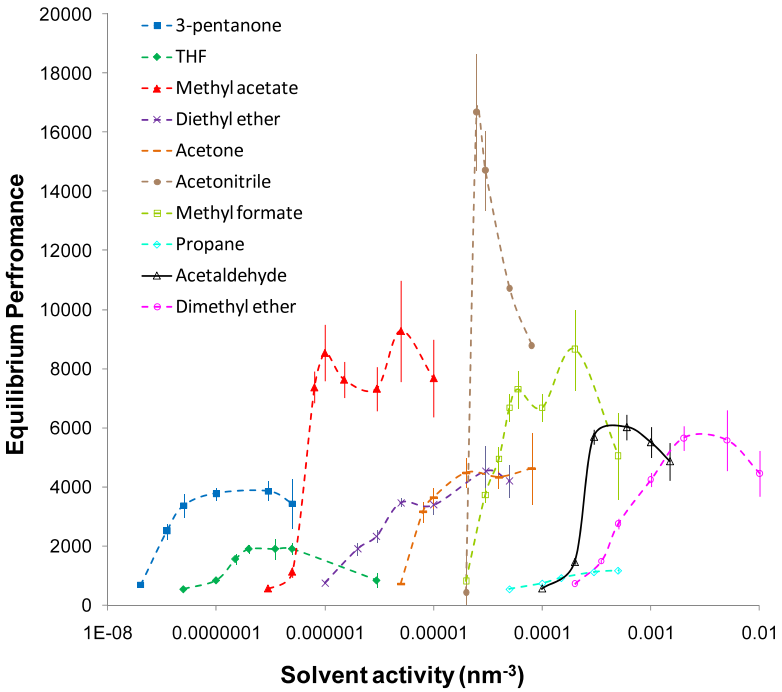

(c)

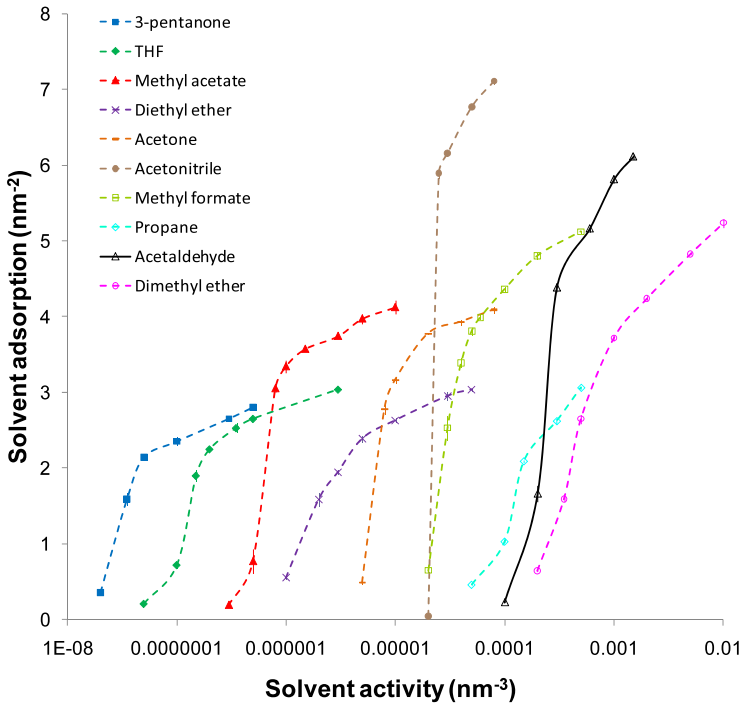

(d)

'equilibrium performance' (EP) here, can be defined as

$$\mathrm{EP} = S_{\mathrm{CO_2}} C_{\mathrm{CO_2}} = \left(\frac{\rho_{a,\mathrm{CO_2}}}{\rho_{b,\mathrm{CO_2}}}\right)^2 \frac{\rho_{b,\mathrm{N_2}}}{\rho_{a,\mathrm{N_2}}} \tag{7}$$

Finally, the absolute specific adsorption is also measured, $N_x = H\rho_{a,x}$.

3.1 Investigation of solvent type

Figures 1a, 1b and 1c show how the selectivity, capacity and EP depend on the solvent activity for each solvent investigated in this work, for the same exhaust gas state (temperature and pressure are 298.15 K and 1.0 bar respectively, with carbon dioxide mole fraction of 0.1) in a graphitic slit

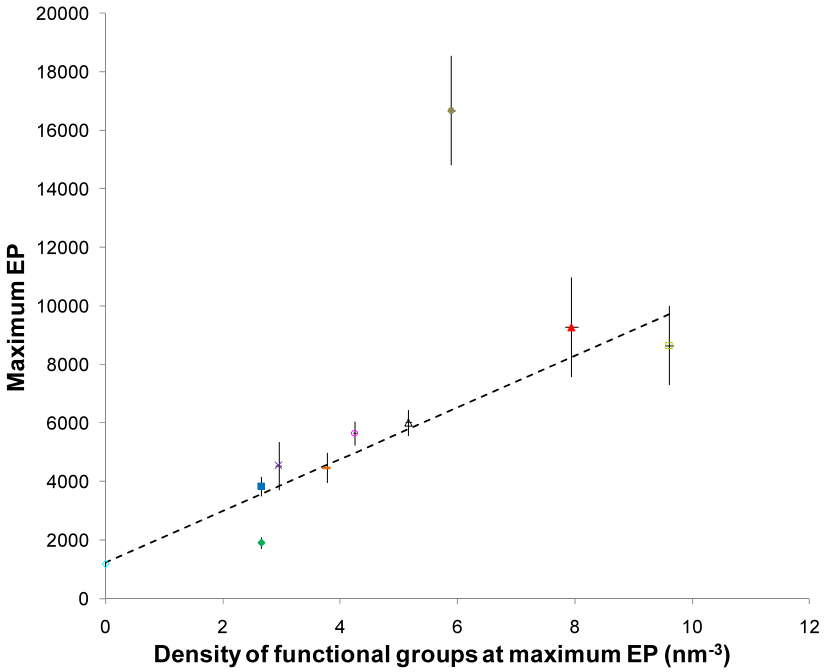

Fig. 2 (Color online) Dependence of the maximum in equilibrium performance on the density of functional groups at this maximum in equilibrium performance for several solvents coadsorbed with the exhaust gas in a 1 nm graphitic pore at 298.15 K. *The colour coding* is the same as for Fig. 1a. Symbols with error bars are simulation results while *the dashed line* is a linear fit to the simulation data (excluding acetonitrile)

pore of width 1.0 nm. Note that the solvent activity is defined here as $\gamma = \exp(\mu_s^*/k_BT)$, where μ_s^* is the configurational contribution to the solvent chemical potential (and k_BT = Boltzmann's constant times the temperature), and hence tends to the solvent density in the limit of low density. Figure 1d shows the corresponding surface density of solvent molecules.

For each solvent we find similar behaviour. At low solvent bulk density there is little impact on the adsorption of either carbon dioxide or nitrogen within the pore, as expected. However, as the solvent bulk density is increased, and hence as solvent specific adsorption increases (see Fig. 1d), we find that all of these performance measures can increase substantially. For some solvents these measures increase dramatically, indicating that pore-filling might occur via capillary condensation (although the existence of metastable branches of the isotherms has not been investigated here). For each solvent, the selectivity increases monotonically, albeit unevenly in some cases, with solvent partial pressure. On the other hand, capacity always reaches a maximum at a specific partial pressure for each solvent. These two measures counteract each other to produce, in general, a plateau in EP over a limited range of solvent partial pressure. Acetonitrile has distinctive behaviour in this respect in that a sharp peak in EP, rather than a plateau or broad peak, is observed. This might be related to the very sharp increase in specific acetonitrile adsorption with activity at this point (see Fig. 1d), which strongly indicates a capillary condensation transition.

At sufficiently high solvent partial pressure capacity decreases much faster than selectivity increases for all solvents, resulting in a steady reduction in EP after the plateau region. So, for each solvent there is a 'window of opportunity' in the solvent partial pressure, equivalent to about one decade in pressure, for which the EP reaches a plateau and is greater than 1, although the minimum and maximum pressures corresponding to this window are different for each solvent. This general behaviour agrees with that observed using the simple DFT model in paper 1. It confirms that this behaviour is typical and is not an artefact of the simple DFT model used in that earlier work.

Examination of Figs. 1a to 1c shows that propane is the worst of the solvents, and this is caused by the lack of any functional groups. All of the oxygen-containing solvents are superior. The best solvents appear to be the esters methyl formate and methyl acetate, which each have two oxygen atoms, and acetonitrile. In fact, the trends in EP observed here correlate nearly linearly with the density of solvent oxygen groups in the slit pore. Figure 2 plots this density for each solvent at maximum EP against maximum EP. The dashed line in Fig. 2 is a linear fit to this data for solvents with oxygen groups together with propane. It can be seen that to within statistical error each solvent, except THF and acetonitrile, lies close to this linear trend. We must conclude from this that specific interactions between carbon dioxide and solvent functional groups tend to dominate equilibrium performance. Given that the Lennard-Jones parameters of the oxygen atoms for these solvents are not unusual, this data suggests that it is electrostatic interactions that lead to this behaviour.

Two solvents, THF and acetonitrile, are outliers in Fig. 2 and deserve further comment. First, it should be noted that

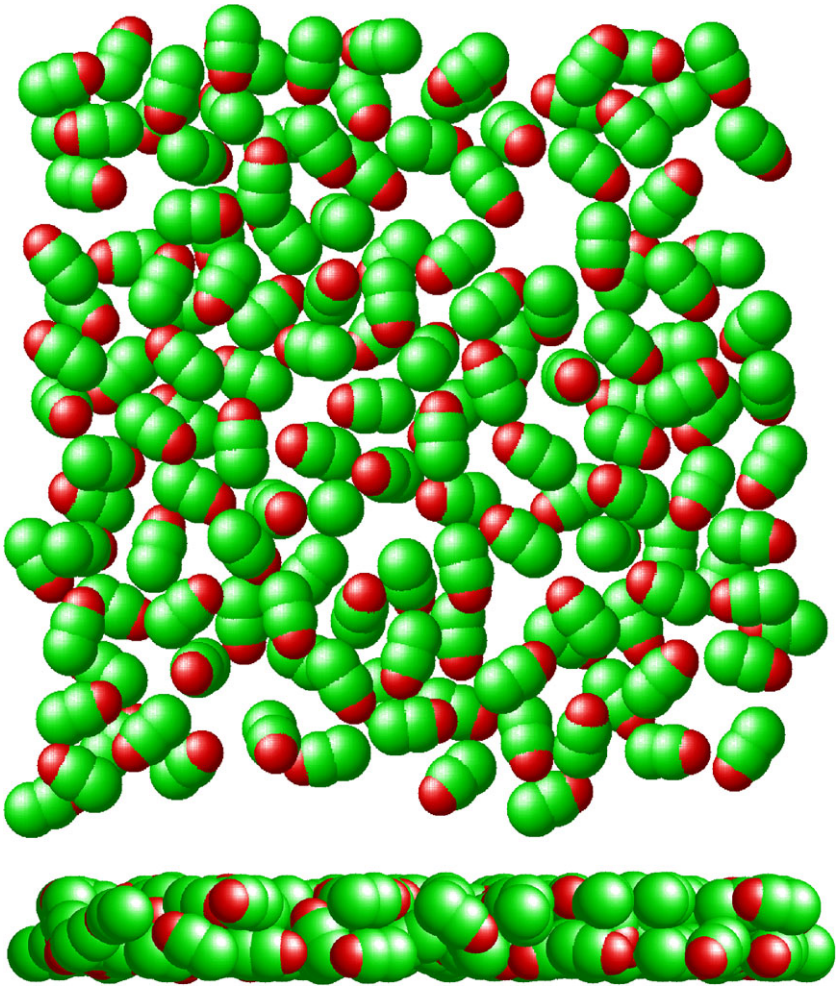

(a)

Fig. 3 (**a**) Typical configuration corresponding to acetonitrile with activity 2.5×10^{-5} nm^{-3} in a 1 nm graphitic pore at 298.15 K. *The lower picture* views this configuration 'edge-on' to illustrate the bilayer nature of this state. Under these conditions acetonitrile improves both the selectivity and capacity of carbon dioxide in the pore due to relatively strong interaction with carbon dioxide and the existence of many small voids. (**b**) As for (**a**), except that the activity of acetonitrile is 1×10^{-4} nm^{-3}. At this state point acetonitrile improves the selectivity but not the capacity of carbon dioxide in the pore because there are fewer voids able to accommodate small gas molecules

the performance for THF observed here in the 1.0 nm pore using an accurate molecular model and essentially exact statistical mechanical treatment is in reasonably good agreement with the behaviour observed using the simple DFT model in paper 1. In that work the peak capacity of about 119 occurred at THF bulk density 1×10^{-7} nm^{-3}, with selectivity equal to 19. In this work we find the peak capacity of about 102 occurs at a THF activity in the region of 1.5×10^{-7} nm^{-3}, with selectivity equal to 15. It is interesting that THF is not a particularly good choice of solvent, despite its good solubility in the bulk liquid phase (the solubility of carbon dioxide in bulk THF is 6.2 cm^3 (STP) cm^{-3} atm^{-1} at 298 K and low pressure while for carbon dioxide in methyl acetate it is 6.0 cm^3 (STP) cm^{-3} atm^{-1}—Bara et al. 2010). The fact that THF has good bulk solubility for carbon dioxide yet performs poorly in a 2-dimensional slit-pore environment might be a consequence of geometric factors. In the bulk liquid phase THF is known (Bowron et al. 2006) to have a tendency to generate small voids due to the packing arrangement of plate-like THF molecules. However, within a slit-pore THF molecules tend to orient parallel to the pore, largely eliminating the chance to form these small voids. Instead, the plate-like THF molecules tend to form a disordered hexagonal arrangement that is unlikely to form small voids to the same extent. Turning to acetonitrile, it is clearly the best of these solvents, with its peak EP (16674) being about 8.8 times that of THF modelled here (1900), and about 6.4 times better than that of THF modelled using the DFT model in paper 1 (2618). The good performance of acetonitrile seen here is mirrored by its good performance for bulk solubility as well (7.1 cm^3 (STP) cm^{-3} atm^{-1} at 298 K and low pressure—Bara et al. 2009).

That the capacity of carbon dioxide in the presence of solvent can be greater than the capacity without solvent in these 1.0 nm pores, even if only for a limited window of solvent partial pressure, is perhaps surprising. To understand how this can happen it is useful to examine typical configurations of appropriate simulations. Figures 3a and 3b display snapshots taken from simulations with acetonitrile activities of 2.5×10^{-5} and 1×10^{-4} nm^{-3} respectively, without

Fig. 3 (*Continued*)

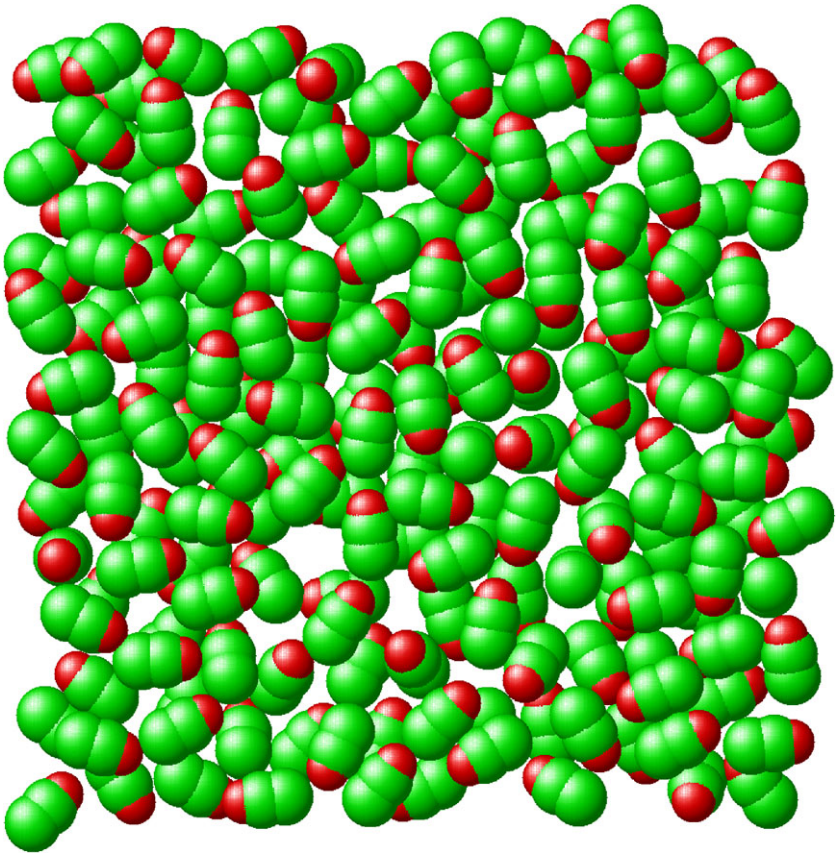

(b)

any exhaust gas. We should expect these states to be similar to those in Fig. 1b corresponding to peak capacity and low capacity (when the pore is full of acetonitrile) respectively, although no exhaust gas is present in these snapshots. In Fig. 3b we see that acetonitrile forms a dense liquid-like phase in the pore that would prevent exhaust gas from entering the pore. However, in Fig. 3a we see that acetonitrile has a sufficiently low liquid-like density that many small voids able to accommodate small gas molecules are formed.

3.2 Effect of pore width

It is well known that the distribution of pore sizes is central in determining the performance of adsorbents. However, the effect of pore size is not known in the particular context of this work where a gas mixture is adsorbed together with an absorbing solvent, except for the case of the DFT model in paper 1. In that work it was found that the partial pressure range over which solvent could improve the equilibrium performance depended very strongly on pore width down to $H = 1.0$ nm. Below 1.0 nm in width the optimal partial pressure of THF did not change significantly. In addition, the selectivity, and particularly the capacity, depended significantly on pore width. It was found that CO_2 selectivity always increased when solvent was coadsorbed with the exhaust gas, and that selectivity values in the region of 60 could be obtained for all pore widths studied without compromising CO_2 capacity, except for $H = 1.0$ nm. For this pore width a selectivity of 35 could be achieved without compromising CO_2 capacity. On the other hand, the peak CO_2 capacity steadily decreased with increasing pore width, from about 550 for $H = 0.8$ nm to around 27 for $H = 1.2$ nm.

In the previous sub-section the carbon dioxide selectivity and capacity was studied for an exhaust gas composed of nitrogen and carbon dioxide adsorbed in 1.0 nm graphitic slit-pores together with several different solvents. According to the models used here, the best performing solvent in these pores was found to be acetonitrile, and so in the remainder of this work the focus remains on this solvent. The aim of this sub-section is to investigate the effect of pore width on equilibrium performance using acetonitrile as solvent.

Figure 4a displays the equilibrium performance for acetonitrile coadsorbed with the exhaust gas at 298.15 K in pores of width 0.7, 0.8, 0.9, 1.0 and 1.2 nm. These pores fall within the range commonly defined as 'microporous' (Sweatman and Quirke 2005, 2006) and are expected to have greatest impact on the performance of microporous active

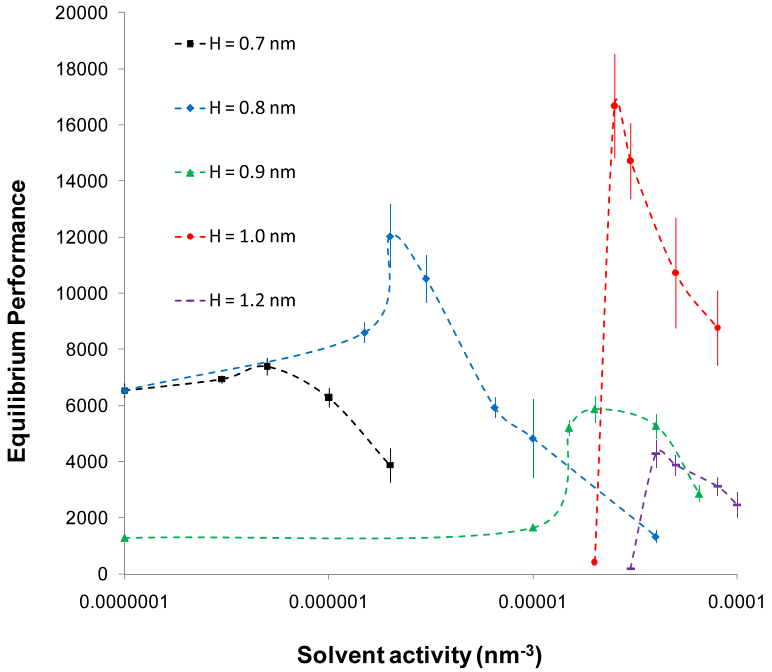

(a)

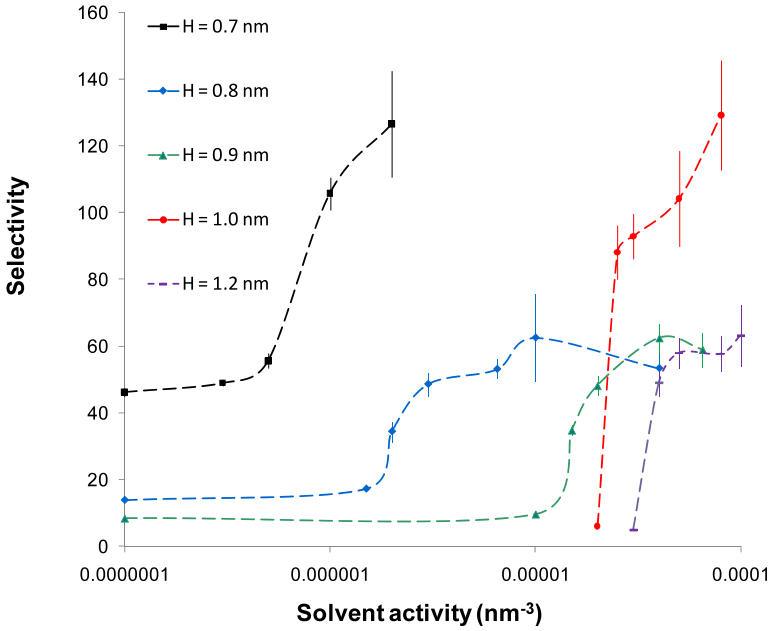

(b)

Fig. 4 (Color online) (**a**) Dependence of the equilibrium performance on solvent activity for coadsorption of acetonitrile and the exhaust gas in pores of different widths at 298.15 K. The pore widths from left to right are 0.7 nm (*black squares*), 0.8 nm (*blue diamonds*), 0.9 nm (*green triangles*), 1.0 nm (*red circles*), and 1.2 nm (*purple horizontal bars*). Solvent activity is plotted on a logarithmic scale, and the EP for $H = 0.7$ nm has been divided by 10. Symbols with error bars are simulation results while *dashed lines* are a guide to the eye. (**b**) As for (**a**), except the selectivity is plotted. (**c**) As for (**a**), except capacity is plotted (the capacity for $H = 0.7$ nm has been divided by 10). (**d**) As for (**a**), except the absolute specific solvent adsorption is plotted. (**e**) As for (**a**), except the absolute specific CO_2 adsorption when adsorbed alone (see text) is plotted. *The left and right vertical dotted lines* indicate the CO_2 activity used to obtain results in (**a**) (1 bar) and Fig. 6 (10 bar) respectively

carbons under these conditions. Note that the equilibrium performance for $H = 0.7$ nm has been divided by 10 to ensure it can be displayed conveniently on the same plot as other pore width data. Figure 4b displays the selectivity, Fig. 4c the capacity, and Fig. 4d the absolute specific solvent adsorption resulting from the same simulations. To provide a benchmark for this analysis Fig. 4e shows the absolute specific adsorption for CO_2 when adsorbed alone in these pores.

Interestingly, these EP results are qualitatively quite different to those predicted by the simple DFT model in paper 1. Although for each pore width we observe the same characteristic peak behaviour in EP, the dependence of the location (in terms of solvent activity, or partial pressure) of the maximum in EP on pore width is quite different to that observed in paper 1. In contrast to paper 1, where the peak EP occurred at a similar solvent partial pressure for $H = 0.8$ and 1.0 nm pores, here we find that the location

Fig. 4 (*Continued*)

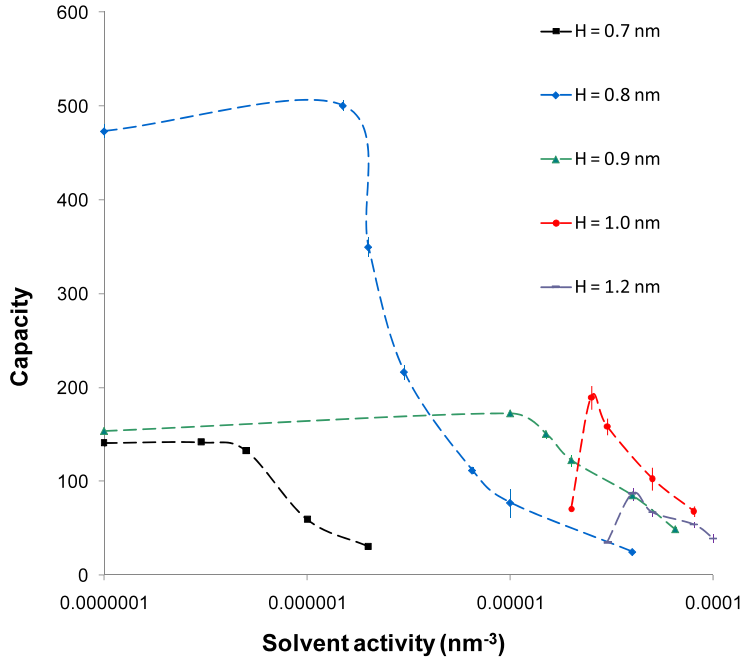

(c)

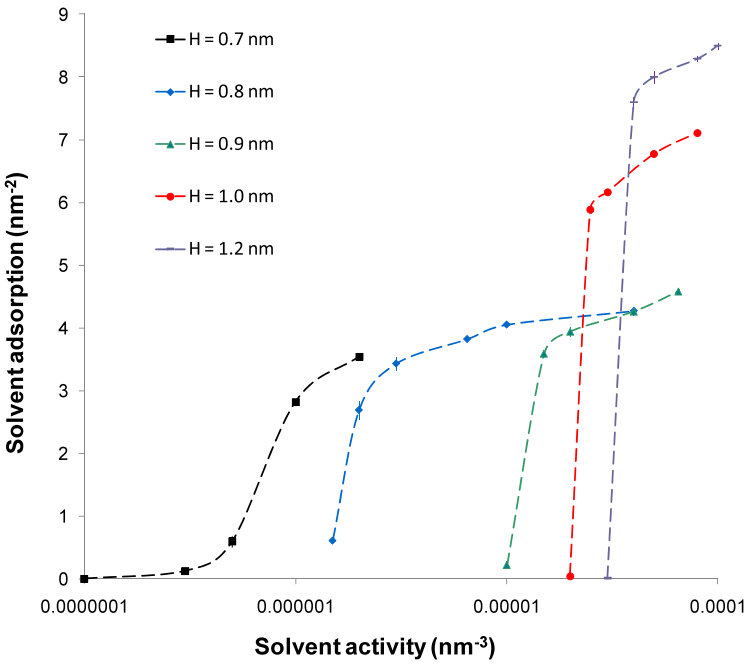

(d)

is similar for $H = 0.9$ to 1.2 nm pores, which means that choosing an acetonitrile activity of 4×10^{-5} nm^{-3} (roughly equivalent to 1.65 mbar) would be sensible for a material with this combination of pores. On the other hand, the activity corresponding to maximum EP changes dramatically for $H = 0.7$ and 0.8 nm pores, being roughly 2×10^{-6} and 5×10^{-7} nm^{-3} respectively. It is suggested that this difference in behaviour (between this work and paper 1) is a result of using accurate molecular models here, compared to spherical models in paper 1, that in the narrowest pores can align with the pore direction to increase their external potential energy. On the other hand, the dependence of the magnitude of maximum EP with pore width does broadly agree with that observed in paper 1. That is, we generally see a dramatic reduction in maximum EP with increasing pore width. However, there is an exception for acetonitrile

Fig. 4 (*Continued*)

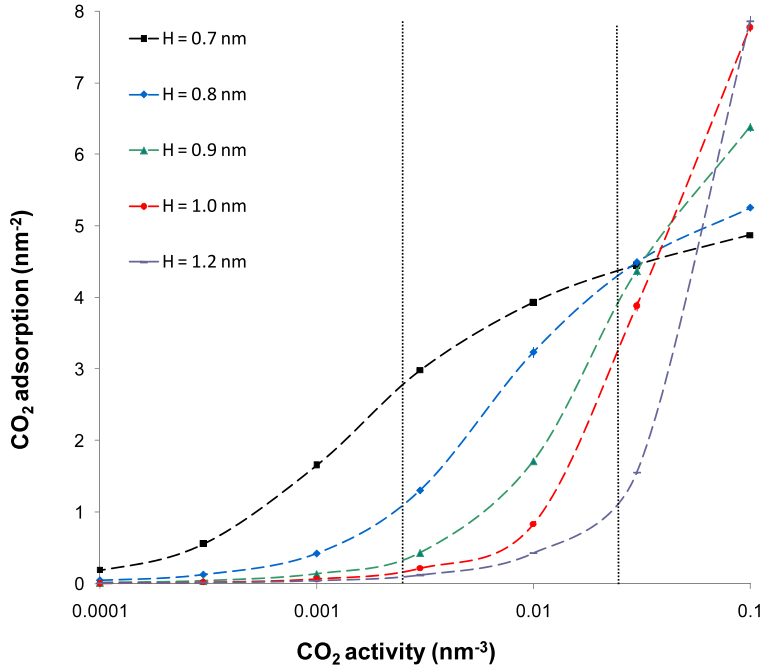

(e)

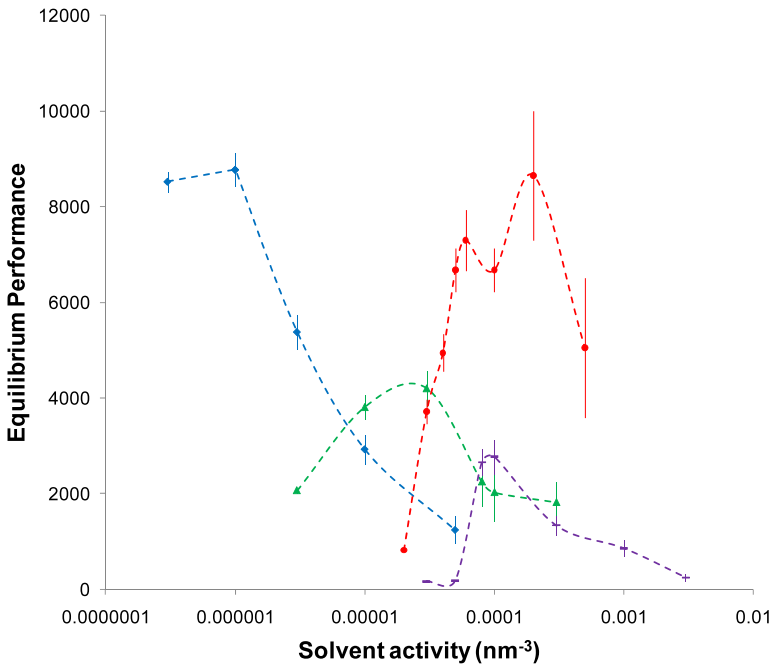

Fig. 5 As for Fig. 4a, except that data corresponds to methyl formate as solvent, and no data is provided for $H = 0.7$ nm pores

at $H = 1.0$ nm, for which the maximum EP is greater than for $H = 0.8$ and 0.9 nm, and is second only to $H = 0.7$ nm. This peak in maximum EP with pore width at $H = 1.0$ nm is likely to be caused by formation of a bi-layer in the 1.0 nm pore, that does not occur in the other pores analysed here, due to favourable packing of two layers of acetonitrile in pores of this width, compared to pores of other widths, as shown in Fig. 3a. Due to this favourable packing the density of functional groups with which CO_2 interacts is strongly increased, compared to neighbouring pore widths. This effect can be observed in Fig. 4d which shows the absolute adsorption of solvent molecules for each pore width as solvent activity increases in the presence of the exhaust gas. A similar effect, i.e. favourable packing in pores of width $H = 1.0$ nm leading to improved EP compared to other pores, is also observed for methyl formate, as shown in Fig. 5.

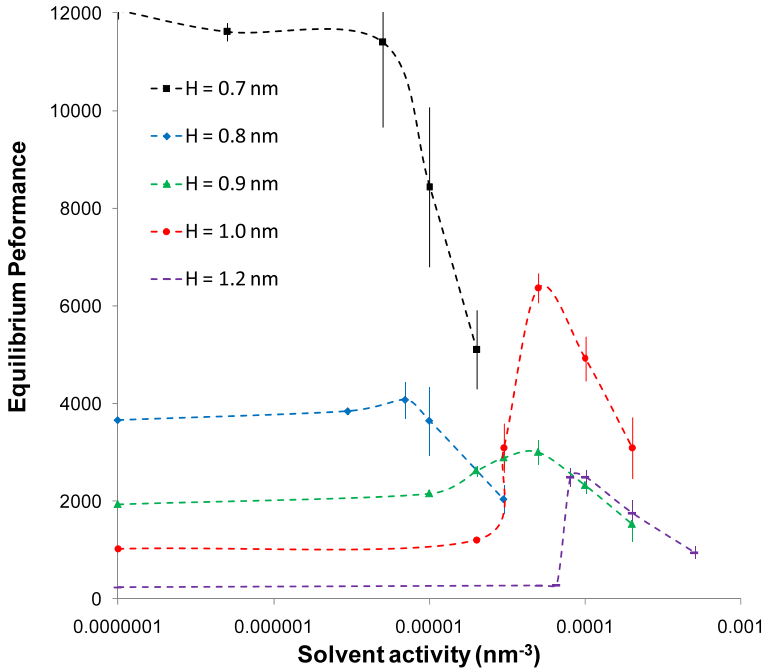

Fig. 6 (Color online) Dependence of equilibrium performance on solvent activity for coadsorption of acetonitrile and the exhaust gas at higher pressure (see text) in pores of different widths at 298.15 K. The pore widths from left to right are 0.7 nm (*black*), 0.8 nm (*blue*), 0.9 nm (*green*), 1.0 nm (*red*), and 1.2 nm (*purple*). *Circles* with error bars are simulation results while *dashed lines* are a guide to the eye

Comparison of Figs. 4b and 4c shows that the peaks in EP observed in Fig. 4a for $H = 0.7$, 0.8 and 0.9 nm are largely due to an increase in selectivity, not capacity. However, for $H = 1.0$ and 1.2 nm increases in both selectivity and capacity lead to increased EP.

Figure 4e shows how CO_2 adsorption varies with pore width and CO_2 activity when CO_2 is adsorbed alone in each pore. The vertical dotted lines correspond to the CO_2 activities used to produce Figs. 4a and 6 for 1 bar and 10 bar exhausts respectively. In order to obtain CO_2 adsorption corresponding to the peak capacity for 1.0 nm pores in Fig. 4c, the CO_2 activity for pure adsorption of CO_2 would need to be nearly triple that of the activity of CO_2 in the 1 bar exhaust. In other words, for 1.0 nm pores the effect on CO_2 adsorption of adding acetonitrile with activity 2.5×10^{-5} nm^{-3} to the 1 bar exhaust is similar to tripling the exhaust gas pressure. A similar effect is seen for 1.2 nm pores. However, for pores smaller than 1.0 nm we see the opposite effect, i.e. the CO_2 capacity is slightly less at maximum EP than when there is no solvent at all.

The result of this analysis is that a more complex picture has emerged regarding the effect of pore size on equilibrium performance than was previously known. Essentially, the value of this process (in terms of equilibrium performance at least) is very sensitive to the pore-size distribution of any given porous material. This suggests that it is also likely to be sensitive to the nature of fluid-solid interactions. For porous materials dominated by the very smallest pores, i.e. $H = 0.7$ nm in width here, we see from Fig. 4a that there is unlikely to be much gained by adopting this process. Only a very slight increase in equilibrium performance is seen for this pore width when solvent is added. On the other hand, for materials whose adsorptive performance is dominated by larger pores this process could result in a much improved equilibrium performance. It is useful to consider a simple example at this point. Suppose, for example, that an active carbon consisted of equal areas of pores with widths 0.7, 0.8, 0.9, 1.0 and 1.2 nm, and that this material was used to separate an exhaust gas identical to that examined in this work. The methods used in this work would predict that when acetonitrile with partial pressure of 1.65 mbar was coadsorbed with the exhaust gas the material's equilibrium performance would be about 0.63 times that when no solvent was used, i.e. significantly worse. However, if we consider the same material, but now without any 0.7 nm pores, the equilibrium performance would be 3.8 times better with solvent than without. Moreover, if we consider a hypothetical templated porous material that consists only of 1.0 nm pores then, according to the results in Fig. 1c, its equilibrium performance could be improved by a factor of nearly 40 with the addition of acetonitrile solvent. Clearly, the 0.7 nm wide pores dominate equilibrium performance for this carbon capture application.

3.3 Effect of pressure

Pressure is one of the key variables to be optimised when designing a pressure swing adsorption separation process. So, this sub-section will investigate the effect of increased exhaust gas pressure on the equilibrium performance of the proposed process. Specifically, an exhaust gas at the same temperature (298.15 K) as before but where the activity of

both nitrogen and carbon dioxide are ten times larger will be considered. This exhaust gas mixture would have very nearly the same composition (CO_2 mole fraction = 0.1) and a pressure nearly ten times the one previously studied, i.e. about 10 bar. This pressure is very unlikely to be used for a carbon capture process because of the wasted energy and cost associated with compressing nitrogen in the exhaust, most of which will ultimately be released to the atmosphere. Rather, the aim of this section is a more general investigation of the effect of increased pressure on equilibrium performance.

Once again, the dependence of equilibrium performance on pore width is studied, and the results are plotted in Fig. 6. We see quite similar trends to those seen in Fig. 4a, although there are some significant differences. Overall, we see that the equilibrium performance has been cut nearly in half for most pore widths. Largely, these reductions in EP are due to a reduction in capacity, not selectivity. For the 0.7 nm pores the EP has dropped by much more than half, and we also no longer see a maximum in EP, although there is considerable statistical error in these results. The maximum in EP for 0.8 nm pores has also nearly disappeared. Results for the other pores become more similar to those in Fig. 4a as pore width increases. Interestingly, for these pores (0.9, 1.0 and 1.2 nm) a sensible choice for acetonitrile activity is 8×10^{-5} nm^{-3}, only slightly higher than for the case with the exhaust gas at 1 bar. The reason for this difference in the results for the 1 and 10 bar exhausts is that at 10 bar the smallest pores, 0.7 and 0.8 nm, are full or very nearly full with CO_2 under these conditions. At 1 bar, only the 0.7 nm pore is nearly full. This can be understood by considering the adsorption isotherms in Fig. 4e, and especially CO_2 adsorption for each pore width at each of the vertical dotted lines which correspond to the CO_2 activity for the 1 and 10 bar exhaust scenarios. So, to summarize this section, it is not possible to improve the equilibrium performance of a pore using solvent in this way if it is already full, or nearly full, with CO_2.

4 Conclusion

The equilibrium performance of a novel kind of gas separation process, called 'pressure-swing wetting-layer absorption' here, is analysed using molecular Monte-Carlo simulations of fluid adsorption in graphitic slit-pores. While these simulation results confirm the general behaviour observed using the DFT model of paper 1, i.e. that the equilibrium performance of active carbons might be improved by coadsorption with an absorbent solvent, there are significant differences in detail. Moreover, these simulations have allowed the identification of a suitable test system, i.e. acetonitrile should be tested as the solvent.

The dependence of the optimal solvent partial pressure on pore width is found to be more complex here than observed with the DFT model used in paper 1. With respect to slit-pores and the simple physical solvents here, it appears that equilibrium performance is especially improved in pores that exhibit a bilayer transition. Conversely, gains in equilibrium performance will not be gained where the equilibrium performance is dominated by adsorption in pores that are already filled, or nearly filled, with the gas to be separated.

In addition, theses simulation results have enhanced our understanding of the factors that affect equilibrium performance. As with bulk absorption and selectivity, it is found that the equilibrium performance within a pore depends strongly on both the density of specific solvent groups, the interaction strength of the gases to be separated with these groups, and the structure of the solvent in the porous material. But it is important to note, as was found with THF, that favourable bulk fluid equilibrium performance does not necessarily translate into favourable confined fluid equilibrium performance due to the change in fluid structure under confinement.

With regard to the particular application of carbon capture studied here, we find that the narrowest pores, i.e. 0.7 nm, have the highest equilibrium performance (see Fig. 4a). However, for these narrow pores there is very little advantage in coadsorption with a solvent (see Fig. 4a), and it is likely that a very low (vacuum) desorption pressure will be needed to recover CO_2. For example, in paper 1 for 0.8 nm pores, and exhaust adsorption pressure of 1 bar, and using THF as solvent the desorption pressure to recover most of the adsorbed CO_2 is about 0.01 bar. The 0.7 nm pores in this present work adsorb CO_2 even more strongly, and so even lower desorption pressures are likely to be required. Such low pressures are probably unrealistic for a large-scale process like carbon capture. After the 0.7 nm pores the 1.0 nm pores have the next highest EP when using acetonitrile. The desorption pressure required for these pores is unlikely to be quite so low, and so they probably represent a good compromise. However, this aspect of the process performance has not actually been studied here due to the difficulty of this kind of analysis this when using molecular simulations.

According to the models used here, the equilibrium performance of acetonitrile could be around nine times better than for THF (which was tested in paper 1) for 1.0 nm pores. The partial pressure of acetonitrile should be chosen according to the pore-size distribution of the active carbon tested. But, results presented here suggest that a material dominated by pores in the region of 0.9 to 1.2 nm in width should be sought and that for this material the partial pressure of acetonitrile is likely to be in the region of just a few millibar if the exhaust gas is at 1 bar and room temperature. Of course, as was mentioned in paper 1, gas exiting from this process,

both the purified nitrogen and the captured carbon dioxide, will contain some solvent vapour which should be recovered and recycled. This will incur additional costs which will need to be taken into account in process optimisation studies. In this regard, lower solvent partial pressures would be preferred. For example, from Fig. 1c we might expect methyl acetate to be preferred to acetonitrile if solvent recovery was found to be a dominant cost.

Although the application here is to carbon capture using active carbons, other gas mixtures, materials and solvents could be considered. For example, in the context of carbon capture it might be possible to use the strategy described here together with novel materials such as the nitrogen loaded porous carbons developed by Pevida et al. (2008). As another example, this coadsorption strategy might work well with templated porous materials that have narrow pore size distributions, or with various kinds of nanotube. Alternatively, other kinds of solvent, for example chemical solvents (Heldebrant et al. 2008), might be employed that could enhance the equilibrium performance much further. However, an obvious issue with these solvents is the generation of significant absorption heat. Given the importance of the factors identified, it is interesting to consider the use of ionic liquids as the solvent. These fluids have received considerable attention in recent years (Zhao 2006) for a range of 'green' applications related to their solvation properties, electrical properties, low vapour pressure and other properties. For example, they have been considered (Bara et al. 2009, 2010) as solvents in traditional absorption and membrane-based carbon capture processes. However, their behaviour within nanoporous materials is much less well understood. In terms of the important factors identified here that determine equilibrium performance within a pore, they might perform well in terms of (i) the strength of electrostatic interactions between CO_2 and ionic groups, and (ii) the structure of ionic liquids in confined geometries and particularly the distribution of small voids.

Finally, we need to remember that dynamical issues, such as material transfer and heat generation and transfer, are likely to be very important for the design and operation of a real process, and so the results described here should be considered as indicative. Of course, experimental work is needed to confirm practical feasibility, and detailed process modelling is required for process optimisation. The results here have helped to identify a suitable experimental test system.

References

Bara, J.E., Carlisle, T.K., Gabriel, C.J., Camper, D., Finotello, A., Gin, D.L., Noble, R.D.: Guide to CO_2 separations in imidazolium-based room-temperature ionic liquids. Ind. Eng. Chem. Res. **48**(6), 2739–2751 (2009). doi:10.1021/ie8016237

Bara, J.E., Camper, D.E., Gin, D.L., Noble, R.D.: Room-temperature ionic liquids and composite materials: platform technologies for CO_2 capture. Acc. Chem. Res. **43**(1), 152–159 (2010). doi:10.1021/ar9001747

Bowron, D.T., Finney, J.L., Soper, A.K.: The structure of liquid tetrahydrofuran. J. Am. Chem. Soc. **128**(15), 5119–5126 (2006). doi:10.1021/ja0583057

Briggs, J.M., Nguyen, T.B., Jorgensen, W.L.: Monte-Carlo simulations of liquid acetic-acid and methyl acetate with the OPLS potential functions. J. Phys. Chem. **95**(8), 3315–3322 (1991)

Cracknell, R.F., Nicholson, D., Quirke, N.: A grand-canonical Monte-Carlo study of Lennard-Jones mixtures in slit shaped pores. Mol. Phys. **80**(4), 885–897 (1993)

Fogg, P.G.T., Gerrard, W.: Solubility of carbon dioxide. In: Solubility of Gases in Liquids, p. 253. Wiley, New York (1990a), Chap. 11

Fogg, P.G.T., Gerrard, W.: Carbon monoxide, nitrogen, oxygen and hydrogen. In: Solubility of Gases in Liquids, p. 288. Wiley, New York (1990b), Chap. 13

Frenkel, D., Smit, B.: Understanding Molecular Simulation, 2nd edn. Academic Press, London (2002)

Heldebrant, D.J., Yonker, C.R., Jessop, P.G., Phan, L.: Organic liquid CO_2 capture agents with high gravimetric CO_2 capacity. Energy Environ. Sci. **1**(4), 487–493 (2008). doi:10.1039/b809533g

Pevida, C., Drage, T.C., Snape, C.E.: Silica-templated melamine-formaldehyde resin derived adsorbents for CO_2 capture. Carbon **46**(11), 1464–1474 (2008). doi:10.1016/j.carbon.2008.06.026

Potoff, J.J., Siepmann, J.I.: Vapor-liquid equilibria of mixtures containing alkanes, carbon dioxide, and nitrogen. AIChE J. **47**(7), 1676–1682 (2001)

Steele, W.A.: Physical interaction of gases with crystalline solids. 1. Gas-solid energies and properties of isolated adsorbed atoms. Surf. Sci. **36**(1), 317–352 (1973)

Stubbs, J.M., Potoff, J.J., Siepmann, J.I.: Transferable potentials for phase equilibria. 6. United-atom description for ethers, glycols, ketones, and aldehydes. J. Phys. Chem. B **108**(45), 17596–17605 (2004). doi:10.1021/jp049459w

Sweatman, M.B.: Equilibrium behaviour of a novel gas separation process with application to carbon capture. Chem. Eng. Sci. **65**(13), 3907–3913 (2010). doi:10.1016/j.ces.2010.03.016

Sweatman, M.B., Quirke, N.: Gas adsorption in active carbons and the slit-pore model 1: Pure gas adsorption. J. Phys. Chem. B **109**(20), 10381–10388 (2005). doi:10.1021/jp045273f

Sweatman, M.B., Quirke, N.: Modeling gas adsorption in amorphous nanoporous materials. In: Reith, M., Schommers, W. (eds.), Handbook of Computational and Theoretical Nanotechnology, vol. 5, pp. 329–378. American Scientific Publishers, Stevenson Ranch (2006), Chap. 6

Wick, C.D., Stubbs, J.M., Rai, N., Siepmann, J.I.: Transferable potentials for phase equilibria. 7. Primary, secondary, and tertiary amines, nitroalkanes and nitrobenzene, nitriles, amides, pyridine, and pyrimidine. J. Phys. Chem. B **109**(40), 18974–18982 (2005). doi:10.1021/jp0504827

Yeh, I.C., Berkowitz, M.L.: Ewald summation for systems with slab geometry. J. Chem. Phys. **111**(7), 3155–3162 (1999)

Zhao, H.: Innovative applications of ionic liquids as "greem" engineering liquids. Chem. Eng. Commun. **193**(12), 1660–1677 (2006). doi:10.1080/00986440600586537

Zhao, X.C., Leng, Y.S., Cummings, P.T.: Self-assembly of 1,4-benzenedithiolate/tetrahydrofuran on a gold surface: a Monte Carlo simulation study. Langmuir **22**(9), 4116–4124 (2006). doi:10.1021/la0532252